

Is superorbital modulation in SMC X-1 caused by absorption in warped precessing accretion disc?

PRAGATI PRADHAN,^{1,*} CHANDREYEE MAITRA,² AND BISWAJIT PAUL³

¹*Massachusetts Institute of Technology, Kavli Institute for Astrophysics and Space Research, 70 Vassar St., Cambridge, MA, 02139, USA*

²*Max Planck Institute For Extraterrestrial Physics, 85748 Garching, Germany*

³*Raman Research Institute, Astronomy and Astrophysics, C. V. Raman Avenue, Bangalore 560080. Karnataka India*

ABSTRACT

We present a broadband spectral-timing analysis of SMC X-1 at different intensity states of its super-orbital variation using 10 *Suzaku* and 6 *NuSTAR* observations. The spectrum in all the states can be described by an absorbed powerlaw with a high energy cutoff and a black-body component along with an iron emission line. Compared to other supergiant HMXBs, the Fe K α line equivalent width is low in SMC X-1 - from less than 10 eV in high state to upto ~ 270 eV in the low states. The spectral shape is dependent on flux with the hard X-ray spectrum steepening with increasing flux. We also report a highly variable normalisation of the power-law component across these 16 super-orbital states. Pulsations in the hard X-rays for both the instruments were detected in all but two observations. The pulse profiles are near sinusoidal with two peaks and the relative intensity of the second peak decreasing with decreasing luminosity. These findings suggest that the super-orbital modulation in SMC X-1 is not caused by absorption in precessing warped accretion disc alone and there are intrinsic changes in X-rays emanating from the neutron star at different super-orbital states. We also note a putative cyclotron line at ~ 50 keV in the *NuSTAR* spectra of three bright states indicating a possible magnetic field of $\sim 4.2 \times 10^{12}$ G. Finally, with the new pulse period measurements reported here, the time base for the secular spin-up of SMC X-1 is increased by thirteen years and the complete pulse period history shows a sudden change in the spin-up trend around 1995.

1. INTRODUCTION

Super-orbital periods are long term periodic/quasi-periodic intensity variations at timescale often several times the orbital period seen in X-ray binaries (an optical companion with a compact object). For X-ray binary systems with an accretion disk (e.g., LMC X-4), this super-orbital modulation is ascribed *ad-hoc* to the presence of a precessing warped accretion disk (PWAD). These warps in the accretion disk may be caused by an interplay of tidal force (from the companion star), viscous drag of different layers of accretion disk and driven by the intense radiation pressure from the compact object (Larwood 1998; Ogilvie & Dubus 2001). As these warps precess with the disk rotation and cause obscuration of the X-rays from the compact object, we see X-ray intensity variations with super-orbital periodicity.

On the other hand, some objects, especially those (but not limited to) that accrete via stellar wind, such super-orbital modulations are thought to occur due to changes in mass-loss rate, $\Delta\dot{M}$ (which subsequently change the accretion rate on to the compact object). There have been many explanations as to what causes such variable $\Delta\dot{M}$. For example, oscillations in companion stars can cause such variability in $\Delta\dot{M}$ (Koenigsberger et al. 2006) and subsequent variation in X-ray luminosity - provided there is a mechanism to keep such oscillations stable (Farrell et al. 2008). Other possibilities for super-orbital modulation include the existence of corotation interaction regions (CIRs, e.g., in IGR J16493-4348; Bozzo et al. 2017), accretion bulge formed by collision of the stellar wind with the outer edge of the PWAD (Zdziarski et al. 2009), or the formation of a transient disk (e.g., in 4U 0114+65; Hu et al. 2017), magnetic axis precession (where compact object is a neutron star, e.g., Her X-1; Postnov et al. 2013), presence of a third body, or even jet formation (e.g., SS 433, Margon 1984). Furthermore, new discoveries of super-orbital modulation from in all kinds of accreting systems (Supergiant Fast X-ray Transients; SFXTs, classical supergiant X-ray binaries; SgXBs, black hole; BH, Ultra-Luminous X-rays; ULXs) independent of the inclination angles indicate that this effect of super-orbital modulation is not caused by viewing geometry alone (Corbet & Krimm 2013). For an review on this topic, we refer the reader to Kotze & Charles 2012; Corbet & Krimm 2013 and references therein.

* pragati@mit.edu

In this paper, we will investigate the possible cause(s) for super-orbital modulation in another high-mass X-ray binary, SMC X-1. SMC X-1 is an eclipsing binary system discovered in 1971 (Price et al. 1971) located in the Small Magellanic Cloud at a distance of ~ 60 kpc (Neilsen et al. 2004). The pulsar has a spin period of ~ 0.71 s (Lucke et al. 1976), an orbital period of ~ 3.9 d with a B0 I supergiant as the companion and exhibit superorbital variability with a periodicity in the range of 40-60 d (Gruber & Rothschild 1984; Wojdowski et al. 1998). Given the similarity of SMC X-1 with other sources like Her X-1 and LMC X-4, the superorbital variation in SMC X-1 - like these two sources - was ascribed to the PWAD (Wojdowski et al. 1998). Unlike these two sources however, the superorbital period in SMC X-1 is not periodic but varies within 40-60 d repeating cyclically after ~ 7 years each (Clarkson et al. 2003). Such a variability in the super-orbital period for SMC X-1 can theoretically be attributed to the presence of different warping *modes* in the accretion disk (Ogilvie & Dubus 2001).

It is however interesting to note that long-term ASM (1.3-12 keV) and BATSE (20-100 keV) light-curves of SMC X-1 covering very different energies show similar variations in the super-orbital modulation (Fig. 1 of Clarkson et al. 2003). This similarity in the super-orbital modulation across the entire energy range of 1.3-100 keV cannot be explained if the super-orbital modulation in SMC X-1 is a result of absorption by neutral matter in the PWAD (since soft X-rays are absorbed more than hard X-rays). Such lack of absorption signatures was also reported in the original paper by Wojdowski et al. (1998). Later authors also argue that such a complex super-orbital behaviour in SMC X-1 cannot be understood by assuming simple models of PWAD alone (see Discussions of Clarkson et al. 2003; Trowbridge et al. 2007).

In this paper, we investigate the broad band X-ray spectral and timing characteristics of SMC X-1 at different superorbital phases to examine the proposed scenario of intensity variation by absorption in the precessing warped disk. The X-ray spectrum of SMC X-1 is usually described with two components: a hard power-law component and a soft-thermal component with the latter possibly arising from the reprocessing of soft X-rays (Paul et al. 2002). A remarkable dissimilarity and phase lag of the soft X-ray with the hard X-ray pulse profiles has also been noted in literature (Paul et al. 2002; Neilsen et al. 2004; Hickox & Vrtilek 2005).

The X-ray spectrum of neutron star High Mass X-ray binaries (HMXBs) also usually feature iron $K\alpha$ emission lines which are produced by fluorescence emission of either neutral or partially ionized matter in the accretion disk or circumstellar matter around the neutron star. One interesting aspect of SMC X-1 is its remarkably weak iron line in the X-ray spectrum compared to other supergiant HMXBs (Giménez-García et al. 2015).

In this paper, we present, for the first time, a comprehensive view of the different spectral states of the super-orbital variation of SMC X-1 through simultaneous broadband spectral fitting (and timing analysis) using *Suzaku* and *NuSTAR* observations. In Section 2, we present the details of the observations and data reduction. In section 3, we present the details of data analysis and results followed by discussion in section 4 and finally a summary in section 5.

2. OBSERVATIONS AND DATA REDUCTION

2.1. Suzaku

SMC X-1 was observed with the *Suzaku* observatory (Mitsuda et al. 2007) ten times during 2011-2012. *Suzaku* consists of two main payloads: the X-ray Imaging Spectrometer (XIS, 0.2-12 keV; Koyama et al. 2007) and the Hard X-ray Detector (HXD, 10-600 keV; Takahashi et al. 2007). The XIS consists of four CCD detectors of which three (XIS 0, 2 and 3) are front illuminated (FI) and one (XIS 1) is back illuminated (BI). The HXD comprises PIN diodes and GSO crystal scintillator detectors.

The data reduction was done on the filtered ‘cleaned’ event files following the reduction technique mentioned in the same *Suzaku* ABC guide¹. We applied the barycentric correction to all event files using *aepipeline*. In case of CCD data as obtained by XIS, we had to investigate the effect of pile-up which is two photons of lower energy being read as one with higher energy, thereby causing artificial hardening of the X-ray spectrum. Therefore, for those observations affected by pile-up, we discarded photons collected within the portion of the PSF where the estimated pile-up fraction was greater than 4 % determined using the FTOOLS task *pileest*. XIS lightcurves and spectra were then extracted by choosing circular regions of $\sim 3'$, or $4'$ radius from the source position depending on whether the observation was made in 1/4 or 0 window mode, respectively. Background for the XIS were extracted by selecting regions of the same

¹ <http://heasarc.gsfc.nasa.gov/docs/suzaku/analysis/abc/>

size as mentioned above in a portion of the CCD that was not significantly contaminated by the source X-ray mission. Being a photon counting detector, data from PIN detector have to be corrected for deadtime which is the time interval for which the detector electronics are processing one photon and thus cannot yet detect the arrival of another. This dead time correction was done using FT00LS task `hxdtdcor`. For the HXD/PIN, simulated ‘tuned’ non X-ray background event files (NXB) corresponding to the month and year of the respective observations were used to estimate the non X-ray background²(Fukazawa et al. 2009).

The XIS spectra were extracted with 2048 channels and the PIN spectra with 255 channels. Response files for the XIS were created using the CALDB version ‘20150312’. For the HXD/PIN spectrum, response files corresponding to the epoch of the observation were obtained from the *Suzaku* guest observer facility³. The observation details are presented in Table 1. For brevity, in this paper, we denote each observation by the last two numbers of its OBSID (eg, 706030010 is denoted by 10), except 706030100 which is abbreviated as 100. The observations 10, 20, 50, 70, 80,90 were in high states (H), 30, 100 in medium (M) and 40, 60 in low states (L).

2.2. NuSTAR

SMC X-1 was observed with *NuSTAR* (*The Nuclear Spectroscopic Telescope Array* ; Harrison et al. 2013) six times during 2012-2016 at various superior orbital phases (reported in Table 1). *NuSTAR* consists of two focal plane modules, FPMA and FPMB, each made up of four pixelated detectors (DET0-DET3) spanning an energy range of 3-79 keV. We used `nupipeline` version 0.4.6 to generate cleaned event files which also provides the recommended source and back ground regions⁴. We extracted the source spectrum and background spectrum using these corresponding region files. Further, we filtered for good time intervals (GTIs) for the duration of the simultaneous observations in FPMA and FPMB.

Finally, following the same naming convention as *Suzaku* , we short-hand the six *NuSTAR* observations by the last two digits of their OBSID. For example, 30202004008 is denoted as 08, 30202004002 as 02 and so on. The observations 08, 02, 03 were in high state (H), 04 in medium (M) and 01, 06 in low state (L).

3. ANALYSIS AND RESULTS

3.1. Timing analysis

In order to get an overview of the long-term superior orbital intensity variation in these 16 observations, we plotted the one-day binned Swift/BAT lightcurve filtered for eclipses and ingresses/egresses of the NS. This is shown in Fig. 1 where we also mark the *Suzaku* and *NuSTAR* observations. Note that we removed the error bars in these lightcurves to assist visual clarity.

3.1.1. *Suzaku* timing analysis

For timing analysis with *Suzaku* data, we extracted background subtracted light curves from the available XIS and PIN barycentric corrected event files. Since the spin period of SMC X-1 is ~ 0.7 s and the lowest available observation mode for XIS was 1/4 window that collect data at 2s interval, we could not use the XIS lightcurves to detect pulsations. The PIN lightcurves were background subtracted by generating a background lightcurve using the simulated background files⁵(Fukazawa et al. 2009). We use the background corrected PIN data extracted with a resolution of 0.01 s to search for periodicity in the individual observations and creation of lightcurves after relevant orbital corrections. In order to correct for Doppler shift of the pulse period due to the orbital motion of the pulsar, we corrected for arrival time in the PIN lightcurves of individual observations using the orbital parameters from Table 3 of Raichur & Paul (2010) extrapolated to the time of each observation.

3.1.2. *NuSTAR* timing analysis

Similarly, to get a combined lightcurve for each *NuSTAR* observation, we add the individual FPMA and FPMB barycenter-corrected (using `barycorr`) lightcurves (binned at 0.01 s). We correct the arrival times of lightcurves for orbital motion using the orbital parameters from Table 3 of Raichur & Paul (2010) extrapolated to the time of each observation - similar to that for the *Suzaku* lightcurves above.

² <http://heasarc.nasa.gov/docs/suzaku/analysis/pinbgd.html>

³ <http://heasarc.nasa.gov/docs/heasarc/caldb/suzaku/>

⁴ <https://heasarc.gsfc.nasa.gov/docs/nustar/analysis/>

⁵ <http://heasarc.nasa.gov/docs/suzaku/analysis/pinbgd.html>

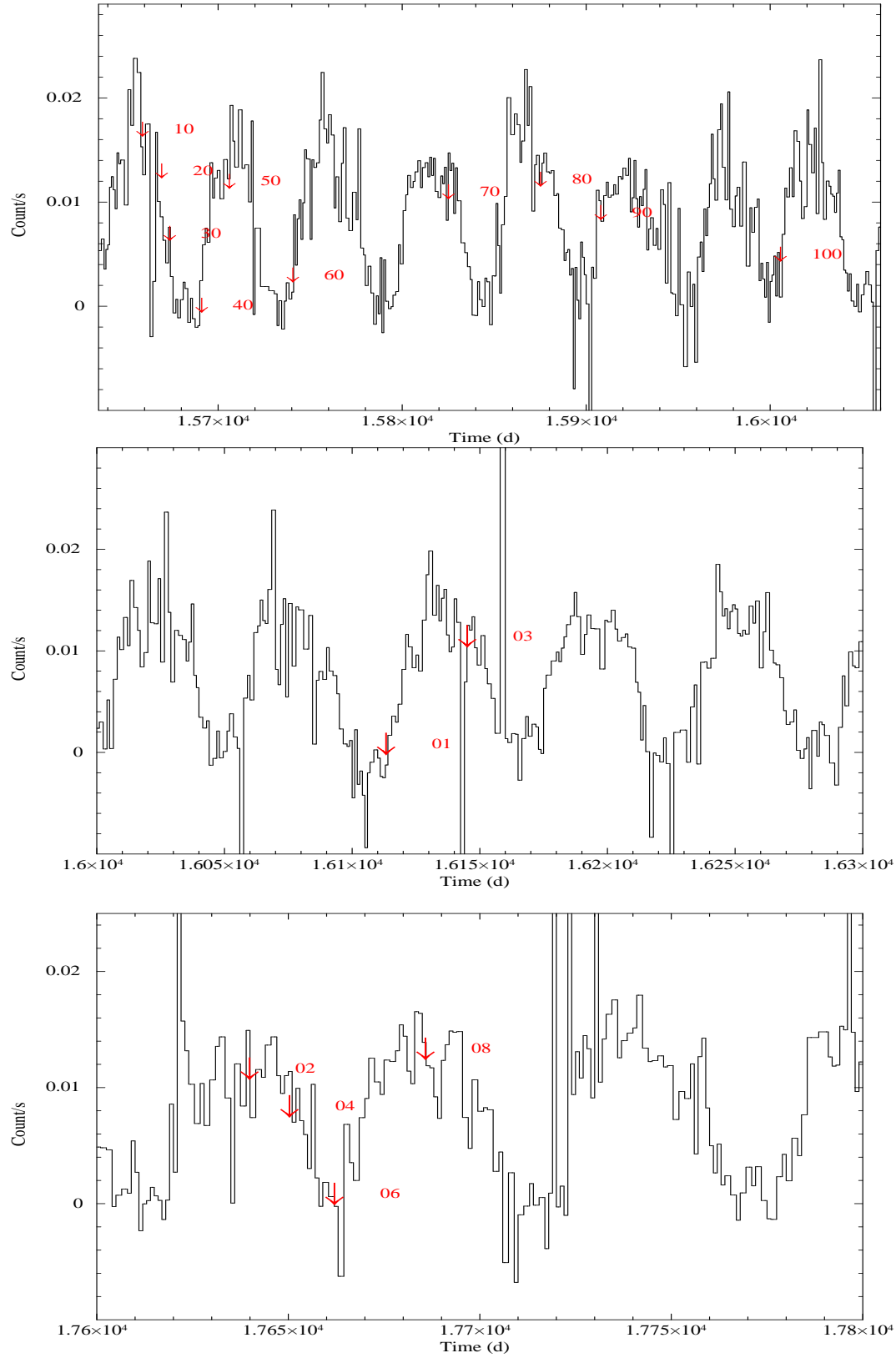


Figure 1. One day binned Swift/BAT lightcurve of SMC X-1 filtered for eclipse and ingress/egresses. Each number in the lightcurve stands for different OBSID of *Suzaku* (top) and *NuSTAR* (middle and below). The figures are marked with aliases of OBSIDs as outlined in Table 1. The errors have been removed for plotting to allow the labelling to be clearly seen.

Table 1. Observation log for SMC X-1 with *Suzaku* and *NuSTAR* ordered in sequentially as decreasing brightness states. The pulse fraction (P.F) is defined as $(P_{max}-P_{UP})/(P_{max}+P_{UP})$ where P_{UP} is the un-pulsed component and P_1 , P_2 are the two peaks. The ratio (R) is $(P_1-P_{UP})/(P_2-P_{UP})$.

Facility	OBSID (alias in this paper)	D.O.O	Useful exposure (ks)	P_{spin} (s)	P.F %	R
<i>Suzaku</i>	706030010 (10)	2011-04-07	18.5	$0.70170860 \pm 0.00000089$	45.8 ± 1.2	0.99 ± 0.04
	706030070 (70)	2011-09-21	18.1	$0.70152930 \pm 0.00000037$	45.9 ± 1.4	1.35 ± 0.06
	706030050 (50)	2011-05-25	17.8	$0.70166090 \pm 0.00000016$	45.3 ± 1.4	1.10 ± 0.05
	706030080 (80)	2011-11-10	19.9	$0.70147950 \pm 0.00000018$	40.1 ± 1.1	0.95 ± 0.04
	706030020 (20)	2011-04-18	17.3	$0.70169900 \pm 0.00000029$	44.7 ± 1.3	1.60 ± 0.07
	706030090 (90)	2011-12-12	17.3	$0.70143900 \pm 0.00000047$	50.6 ± 1.5	1.71 ± 0.09
	706030030 (30)	2011-04-22	15.7	$0.70169140 \pm 0.00000065$	46.9 ± 1.6	2.02 ± 0.14
	706030100 (100)	2012-03-19	18.6	$0.70134440 \pm 0.00000032$	46.5 ± 2.3	1.34 ± 0.11
	706030060 (60)	2011-06-28	18.7	-	< 4.0	-
	706030040 (40)	2011-05-10	17.8	$0.70167570 \pm 0.00000234$	34.4 ± 6.8	2.55 ± 1.58
<i>NuSTAR</i>	30202004008 (08)	2016-10-24	20.1	$0.69953702 \pm 0.00000027$	37.9 ± 0.2	0.99 ± 0.01
	10002013003 (03)	2012-08-06	17.0	$0.70118470 \pm 0.00000006$	36.3 ± 0.3	1.88 ± 0.03
	30202004002 (02)	2016-09-08	20.8	$0.69958702 \pm 0.00000036$	36.1 ± 0.3	1.10 ± 0.01
	30202004004 (04)	2016-09-19	19.9	$0.69957772 \pm 0.00000016$	41.3 ± 0.3	1.67 ± 0.02
	10002013001 (01)	2012-07-05	33.1	$0.70122190 \pm 0.00000068$	12.2 ± 0.6	4.00 ± 1.38
	30202004006 (06)	2016-10-01	19.4	-	< 1.9	-

3.1.3. Pulse profile and pulse period evolution

Pulse profile studies: The spin period search was carried out on the *Suzaku* and *NuSTAR* lightcurves obtained above. Pulsations were clearly detected in nine out of ten *Suzaku* observations and five out of six observations for *NuSTAR*. The best-obtained spin period for each observation are tabulated in Table 1 and a plot of the pulse period history is shown in Fig. 2. There was no clear pulsation in one *Suzaku* observation (60), and one *NuSTAR* observation (06). In order to obtain the pulse profiles for these two observations, we folded the lightcurves at the period corresponding to the highest chisquare value within the period search range. Folded profile from all the observations are shown to the left (*Suzaku*) and right (*NuSTAR*) of Fig. 3. We identify the first ‘broader’ peak as P1 and P2 as the one following it. We notice that although both the peaks evolve with luminosity, the second peak P2 decreases more rapidly with decreasing luminosity. This is especially noticeable in the *NuSTAR* pulse profiles on the right of Fig. 3. In Table 1, we have also listed the ratio (R) of the two peaks P_1 & P_2 above the unpulsed component (P_{UP}) defined as $(P_1-P_{UP})/(P_2-P_{UP})$, and the pulse fraction (P.F) defined as $(P_{max}-P_{UP})/(P_{max}+P_{UP})$.

Pulse period evolution: The pulse period evolution of SMC X-1 has been investigated extensively in the past. Unlike most HMXB pulsars with supergiant companion stars which show both spin-up and spin-down episodes resulting into

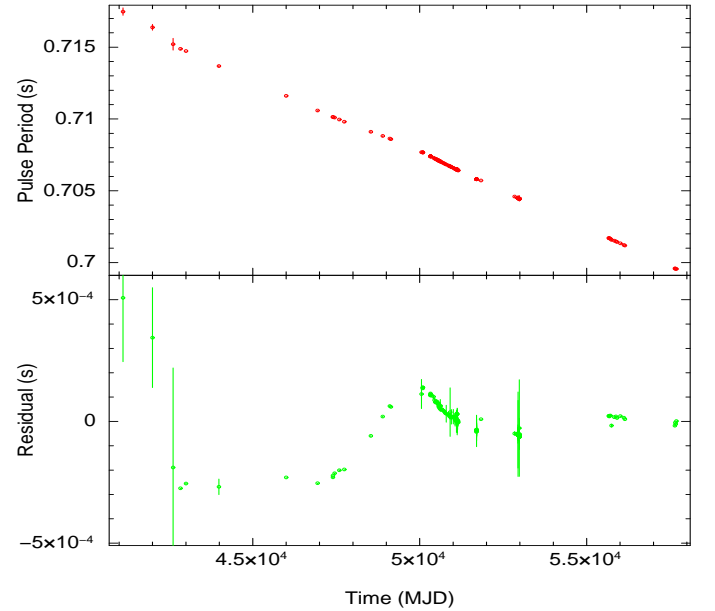


Figure 2. The pulse period history of SMC X-1 is shown in the top panel. Bottom panel shows the residuals after subtraction of a linear fit. A sudden change in the spin-up rate around MJD 50000 is obvious from the residuals.

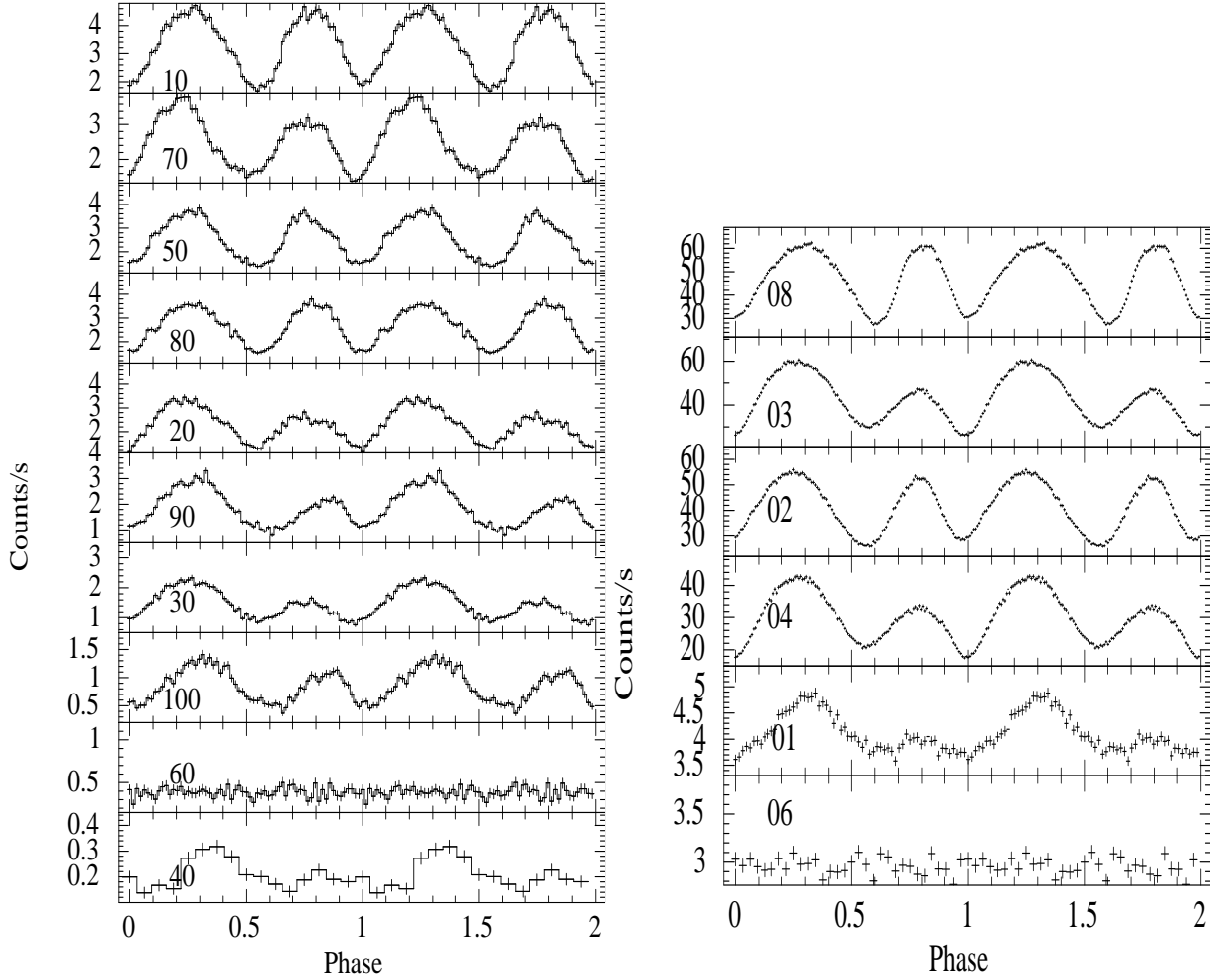


Figure 3. Pulse profiles for all *Suzaku* HXD/PIN (left) and *NuSTAR* (right) observations with the aliases of their OBSID (see Table 1) mentioned in the figures. The pulse profiles are plotted in sequence of their brightness from top to bottom. Note that both the pulse peaks, especially the second peak, P2, show an evolution with luminosity.

significant random variations in period evolution over their long term trends (Bildsten et al. 1997), SMC X-1 has only been found to be spinning up since its discovery. Inam et al. 2010 however, reported some variations in the spin-up rate. Starting from a value of $\sim 3.6 \times 10^{-11} \text{ Hz s}^{-1}$, since its discovery, the spin-up rate halved to a value of $\sim 1.9 \times 10^{-11} \text{ Hz s}^{-1}$ in about 20 years and then increased to $\sim 2.6 \times 10^{-11} \text{ Hz s}^{-1}$ just prior to the launch of RXTE in 1995 since when there are large number of period measurements. A sudden change in the spin-up rate around MJD 50000 is also obvious from the residuals to a linear fit of the period history shown in Fig. 2. We discuss the interpretation of this in details in section 4.

3.2. Spectral analysis

3.2.1. Suzaku

We performed spectral analysis of SMC X-1 using data from XIS-0 and the HXD/PIN. Spectral fitting was performed using XSPEC v12.10.0e. Artificial features are known in the XIS spectra around the Si edge and Au edge and the energy range of 1.75-2.23 keV is usually not used for spectral fitting. For each observation, we fitted the XIS and PIN spectra simultaneously with all parameters tied. The 2048 channel XIS spectra were rebinned by a factor of 10 upto 5 keV, by 2 from 5-7 keV by 14 for the rest. The PIN spectra were binned by a factor of 2 till 22 keV, by 4 from 22-45 keV, and by 6 for the rest to ensure similar signal to noise ratio across the entire energy band.

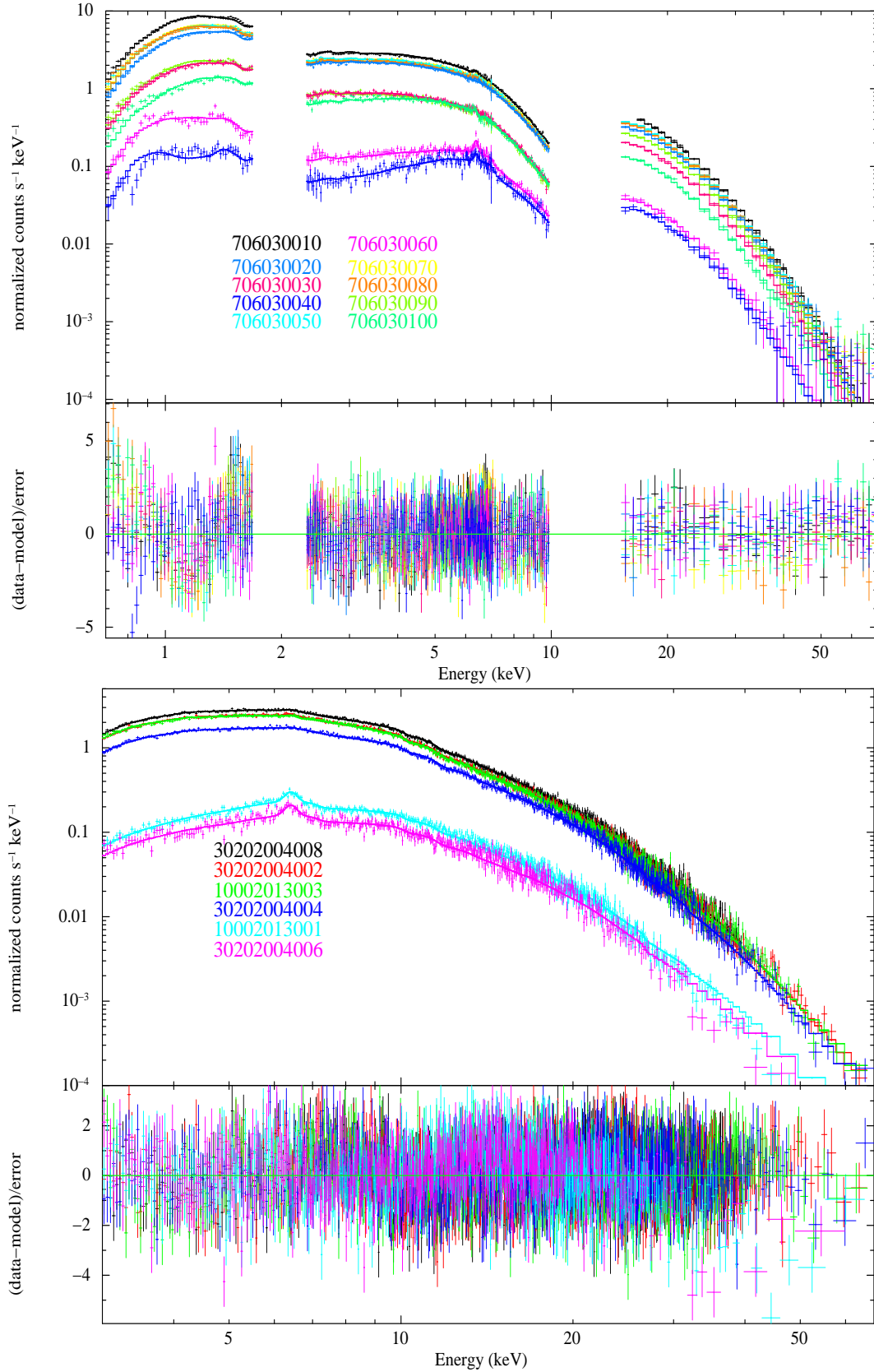


Figure 4. Top: *Suzaku* spectra for all 10 observations plotted together. Below: *NuSTAR* spectra for all 6 observations plotted together. Both these spectra have been fit by an absorbed powerlaw with exponential cutoff energy, a partial ionized absorber and a Gaussian line (plus an additional black body component for *Suzaku*, model 2, section 3.2). The fit parameters of the individual fits for these observations are given in Tables 3 and 4.

We fitted each individual X-ray spectrum of SMC X-1 with standard continuum models⁶ used for NS-HMXBs like an absorbed powerlaw with an exponential cutoff energy, HIGHECUT and CUTOFFPL. Both the models have been used to describe the broad-band spectrum of SMC X-1 in earlier works (Naik & Paul 2004; Pike et al. 2019). In addition to this continuum, the spectra also necessitated a blackbody component to fit the soft excess below 2 keV as seen in many X-ray pulsars (Paul et al. 2002; Hickox et al. 2004), as well as a Gaussian line at 6.4 keV for the K_α emission of neutral iron. The two continuum models described above fitted the X-ray spectra well with the $\chi^2_r/\text{d.o.f}$ for the *Suzaku* spectrum with highest photon counts (706030010) being 1.11/270, and 1.09/271 respectively. We therefore chose the CUTOFFPL model for further spectral analysis. In XSPEC notation, this model (model 1) is:

$$\text{constant} < 1 > * \text{phabs} < 2 > (\text{cutoffpl} < 3 > + \text{bbody} < 4 > + \text{gaussian} < 5 >) \quad (1)$$

The complete set of parameters for the fitting above are listed in Table 2. During the course of the spectral fitting above, we noticed that the change in the X-ray intensity of SMC X-1 at different superorbital phases is not limited to the XIS energy band (0.3-10 keV) alone. The hard X-rays (15-70 keV) measured in the HXD/PIN band also change by a large factor with different superorbital states. This variation is of paramount importance to understand the superorbital modulation in SMC X-1. To the best of our knowledge, such a change in the hard X-ray flux at different phases of superorbital modulation has never been discussed in literature so far, although there have been reports of changes in hard X-ray flux (Table 6 of Brumback et al. 2020) at different superorbital states of SMC X-1.

In the current prevailing hypothesis, the superorbital intensity variation of SMC X-1 is caused by absorption in a precessing warped accretion disk. Such signatures are manifested as a reduction in soft X-rays (below ~ 5 keV) in the low intensity states but the hard X-ray photons should be unaffected by this absorption. Curiously though, we notice that for SMC X-1 in the low super-orbital intensity states, the reduction in soft X-rays are also accompanied by a corresponding decrease in the hard X-ray emission. Such a behaviour is in contradiction with absorption caused by a neutral absorber. A further signature of absorption in neutral medium is the fact that the spectral shape, especially below 3 keV, have a strong energy dependence in soft X-rays (see various examples in Fig. A.1 of Pradhan et al. 2018). The XIS spectra of the *Suzaku* observations of SMC X-1 however do not show any such dependence characteristic of neutral absorption (Fig. 4 top). Motivated by this, we therefore introduced a partially ionized absorber to the above model (say, model 2) which in XSPEC notation is given by the equation below:

$$\text{constant} < 1 > * \text{phabs} < 2 > (\text{zxipcf} < 3 > * \text{cutoffpl} < 4 > + \text{bbody} < 5 > + \text{gaussian} < 6 >) \quad (2)$$

The use of ionized absorber is also justified since such high X-ray luminosity as observed in SMC X-1 contribute to ionization of matter around the neutron star. This is also supported by the remarkably low value of equivalent width

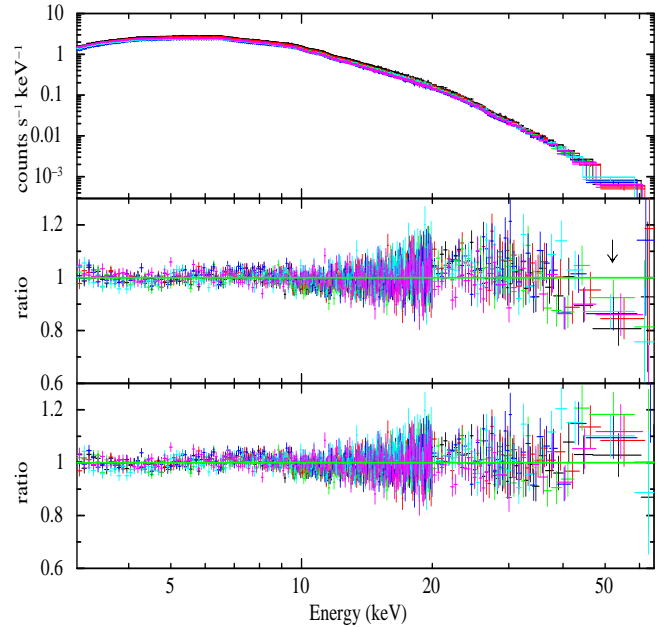


Figure 5. Plot for three *NuSTAR* spectra where a tentative CRSF at ~ 55 keV is spotted (marked with an arrow in middle panel). The middle (lower) panel shows the ratio of data to model without (with) the CRSF model.

⁶ <http://heasarc.gsfc.nasa.gov/xanadu/xspec/manual/XspecModels.html>

of the neutral iron K_α line of SMC X-1 as compared to other similar systems like LMC X-4. The complete set of parameters for the fitting above are listed in Table 3 and individual spectra fit with this model are plotted together on top of Fig. 4.

3.2.2. NuSTAR

We fitted the *NuSTAR* FPMA and FPMB spectra simultaneously with all parameters tied, except the relative instrument normalizations of which were kept free. The 4096 channel FPM spectra were rebinned by a factor of 2 upto 20 keV, by 10 from 20-60 keV by 6 for 60-78 keV and by a factor of 2 for the rest. We use the 3-70 keV *NuSTAR* spectra for spectral fitting using with the same continuum model with partially ionized absorber as *Suzaku*. The only difference being that we did not require any blackbody component to fit the soft excess in contrast to the *NuSTAR* analysis by Pike et al. (2019). (With the sensitivity of *NuSTAR* below 3 keV being very poor, a blackbody component with a temperature of ~ 0.16 keV cannot be constrained with *NuSTAR*). The fits for all the observations are tabulated in Table 4 and the individual spectra are plotted on the bottom of Fig. 4. We also noted an absorption feature in the spectrum reminiscent of a Cyclotron Resonant Scattering Feature (CRSF) around 50-60 keV in the three brightest observations (08, 02, 03) with *NuSTAR*. We used *GABS* to model this cyclotron absorption feature that decreased the $\chi^2/\text{d.o.f}$ from 822/701 to 751/699, 845/700 to 732/698 and 842/700 to 750/698 for observation 08, 02, 03 respectively. The ratio of data to model for these three observations with and without the CRSF component is shown in Fig. 5.

3.3. Joint spectral fitting for different superorbital states

3.3.1. Suzaku

In the prevailing hypothesis for superorbital intensity variation in SMC X-1 (also LMC X-4), the variation is caused by absorption in a precessing warped accretion disk while the intrinsic luminosity of the source remains nearly constant as seen in the soft, ~ 0.1 -10 keV X-ray spectrum (see, e.g., Wojdowski et al. 1998). The nearly constant peak intensity of the super-orbital modulation observed for more than two decades with RXTE-ASM (1.5-12.0 keV band, from 1996-2011), Swift-XRT and MAXI-GSC supports this hypothesis. All of these observations are however well below 20 keV. The aim of this current work is to investigate if the multiple broad band spectra also show evidence of variable absorption.

To achieve this, we performed a joint spectral fitting of the 10 *Suzaku* observations. We first fit the continuum of the brightest observation (10) from both XIS and PIN with an absorbed powerlaw and high energy cutoff coupled with an ionized partial absorber. We then tied all the spectra from other *Suzaku* observations to this model (N_{H1} was frozen at 0.3×10^{22} atoms cm^{-2}) for simultaneous fitting. With this continuum (10) as the reference, we therefore performed joint fitting of the spectra obtained in other intensity states while allowing the absorption parameters, i.e., covering fraction (f), local absorption column density (N_{H2}) and ionization parameter ξ to change.

In case of *Suzaku* where we could constrain the soft excess component, we allowed the black body normalization to vary. Furthermore, we allowed the Gaussian normalization of the 6.4 keV line to change as well. With the above procedure, the low energy part of the spectrum fit considerably well with the low-intensity states exhibiting a higher value of covering fraction. However, the systematic residuals above 10 keV exhibited a misfit in the hard X-ray band. We therefore freed the powerlaw normalization of the 10 spectra which drastically improved the fits. The powerlaw normalization differ by as much as a factor of 6. Seeing such a large change in this powerlaw component, we cross-checked the peak-to-peak superorbital variation in the long-term BAT lightcurves. Interestingly, we find that the peak-to-peak variation of the superorbital modulation in the long-term BAT lightcurves is only $\sim 15\%$. Such a contrast in the powerlaw normalization versus the orbit averaged BAT lightcurves is puzzling and we will discuss this further in section 4.

3.3.2. NuSTAR

For joint fitting of 6 *NuSTAR* observations, we follow the same methodology as above with the same model (without the black body component which cannot be constrained with *NuSTAR*). We fit the spectrum with highest statistics (08) and tied other 5 spectra with this, while allowing the absorption parameters (f , N_{H2} , ξ), powerlaw and Gaussian normalization to be free. We also find the same results as obtained with *Suzaku* and the powerlaw normalization vary by a factor of 6. The physical interpretation of this exercise will be explained in section 4.

This variation of the spectral parameters in both the exercises above as a function of X-ray flux are shown in Fig. 6.

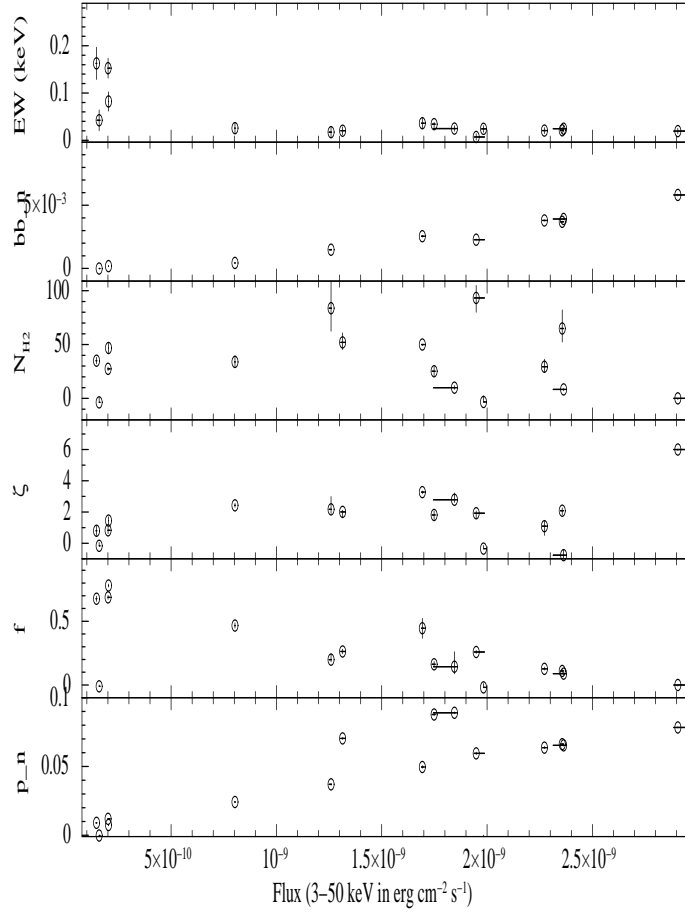


Figure 6. Model parameters versus the 3-50 keV flux corresponding to these 16 observations for joint fits (10 *Suzaku* spectra fit jointly and 6 *NuSTAR* spectra fit jointly) using a powerlaw and an exponential cutoff with a partially ionized absorber, a Gaussian line for neutral iron $K\alpha$ line (and black-body component for *Suzaku* spectra only). For this joint fitting, we allow the black-body, powerlaw normalization, absorption parameters (f , N_{H2} , ξ) and Gaussian normalization to vary. See section 3.3 for details.

4. DISCUSSION

Individual broad band spectra of all observations can be fitted with a **CUTOFFPL**, along with a blackbody for a soft excess (only *Suzaku*) and neutral iron $K\alpha$ line. Equivalent width of the iron line vary from 10-270 eV, anti-correlated with luminosity. Through joint fitting of the 16 spectra in different superorbital states, we find that the powerlaw normalization vary by a factor of upto 6 while the overall variation of the peak of the superorbital modulation obtained from the BAT lightcurves is $\sim 15\%$. In the event of this X-ray variation caused only through absorption in precessing warped accretion disk, the power-law normalisation should not vary beyond the variation in the peak luminosity of the superorbital variation (i.e., upto 15% in case of SMC X-1). This huge difference in the percentage of variation in BAT lightcurves versus powerlaw normalization can only be explained if we introduce an intrinsic variability of X-ray emission from the source as opposed to superorbital modulation caused by absorption⁷

Pulsations are detected in all but two observations of *Suzaku* (15-70 keV) and *NuSTAR* (3-70 keV). We also note that the pulse fraction in hard X-rays (> 12 keV) remain almost constant for 13 out of 16 observations (Table 1). Considerable luminosity dependence is seen in the pulse profile, ratio of the second to the first peaks becomes smaller at lower intensities. This variation of pulse profile morphology also support our hypothesis that there is an intrinsic change in the source spectrum of SMC X-1 with varying super-orbital states.

⁷ Note that taking a cue from the shape of XIS spectrum, the large luminosity of SMC X-1 that ionizes matter, and a very weak iron $K\alpha$ line, we have used an ionized absorber as opposed to neutral.

The timing analysis also reveal that interestingly (except for one *Suzaku* and one *NuSTAR* observation), the lower intensity states in *Suzaku* are also pulsed in hard X-rays. This suggests that perhaps most X-rays travel across the warp instead of being scattered which would otherwise have caused smearing of pulsations. Detection of strong pulsations and relatively low EW of iron line compared to other similar systems indicate that even in the low state we are mostly seeing the central object directly and not in scattered radiation.

From the residuals to a linear fit of the period history shown in Fig. 2, it is obvious that there was a sudden change in spin-up rate around MJD 50000 (year 1995). This abrupt change was also noted from some ROSAT observations, though it was not specifically mentioned in the report (Kahabka & Li 1999). In the scenario that the superorbital intensity variation of SMC X-1 is due to variable absorption, the accretion torque onto the neutron star should be compared against the peak luminosity of the superorbital variation. We therefore compare the peak luminosity before and after the sudden change in spin-up rate (around MJD 50,000). The long term flux variation of SMC X-1 was investigated in detail with HEAO 1 for three cycles and they reported a peak flux of 2.8×10^{-11} erg cm $^{-2}$ s $^{-1}$ in the 13-70 keV band (Gruber & Rothschild 1984). In the current observations with *Suzaku* and *NuSTAR*, some of which are near the peak of the superorbital modulation, the flux in the same energy band is measured to be much higher (Tables 3 and 4), upto a factor 50 compared to the HEAO 1 measurements. It is therefore likely that there was a significant change in the mass accretion rate onto SMC X-1 associated with the change in spin-up rate some time around around MJD 50000 (year 1995). Subsequent to this event, there was a decrease in the superorbital period of SMC X-1 from about 60 days to about 45 days and a weak correlation was found between the superorbital period and the short term spin-up rate (Dage et al. 2019), which may therefore be related to the change in mass-accretion rate. This finding therefore directly support our hypothesis of varying X-ray emission from the source.

It is worthwhile to clarify here that our findings do not question the *presence* of a PWAD in SMC X-1, but rather shows that the *absorption* in the PWAD is not the cause of super-orbital modulation - at least not wholly - and there are signatures of intrinsic changes in X-rays emitted from the neutron star. To reiterate, in the PWAD model, the warped accretion disk is irradiated by the X-rays from the pulsar beam where this hard X-ray photons get reprocessed to soft X-rays. Therefore, by studying the differences in pulse profiles of the direct (hard) and the reprocessed (soft) X-ray emission, constraints can be placed on the disk geometry (Hickox & Vrtillek 2005). Recently, Brumback et al. 2020 used simultaneous XMM-Newton and *NuSTAR* data that span a complete superorbital cycle to illustrate this model. They find that long term changes in soft pulse shape and phase are consistent with reprocessed emission from a precessing inner disk for two (08 and 02 in this paper) out of four observations. In this work too, we note that the variation in soft thermal component clearly map the hard X-rays (black-body versus power-law normalization in Fig. 6) thereby indicating that the hard X-rays are reprocessed, possibly in the accretion disk.

We should also mention here that in observation 04, the same authors note a change in the shape of the *NuSTAR* pulse profiles. Such a change in shape of pulse profiles for obs 04 is also noted in our work (right of Fig. 3) and is one of the evidences that indeed there is some intrinsic change in the hard X-ray emission from the central object. Finally, the authors find no pulsations in observation 06 similar to what is reported here. Such an extinction of pulses (in first half of observation 01) has been explained by Pike et al. 2019 as being caused by obscuration by a Compton thick matter in the accretion disk or inhibition of accretion caused by the onset of propeller regime as seen in the case of Ultra Luminous X-ray sources (ULXs). The latter is ruled out since it is characterized by dramatic flux variability as opposed to ‘continuous’ transition between high and low states like seen in SMC X-1. While the former is still a possibility when we consider scattering of the soft X-rays, it is unlikely that the hard X-rays from the neutron star are scattered enough to switch-off pulsations altogether.

The broad band timing and spectral characteristics of SMC X-1 as reported here from ten *Suzaku* and six *NuSTAR* observations indicate that a variable accretion rate is the possible reason behind the superorbital intensity variation in SMC X-1. Since the X-ray luminosity drives the warp, the configuration of the warp should be sensitive to the mass transfer rate onto the compact object. This possibility of the variable accretion rate is what we have discussed throughly in this paper and have provide many spectral and timing characteristics to solidify our claim that the superorbital modulation is not due to absorption in the precessing warped disk *alone*.

One possible explanation for super-orbital modulation in SMC X-1 drawn analogously from the studies of cataclysmic variables (CVs) is the generation of ‘bright spots’. If the mass transfer rate from the donor star is quasi-steady, the local values of mass transfer in accretion discs can exceed the actual mass transfer rate from the companion star (Rutten et al. 1992). In this scenario, there is a creation of ‘bright spots’ in the accretion disk and the warp in SMC X-1 may transport this mass transfer stream close to the neutron star. As the warp precesses, this bright spot move

through the disc, thus varying the brightness and altering the X-ray spectrum at different super-orbital phases like seen here. Such a possibility although mentioned by earlier authors in literature (Discussion in Clarkson et al. 2003) suffer from a number of drawbacks. In particular, there is no reason to believe that the amount of energy emitted by these bright spots will be a significant when compared to X-rays emitted from the neutron star. Additionally, these bright spots, if present, will be formed well above the co-rotation radius of the accretion disk and is not expected to be pulsed.

In order to gain further insights into the variation of super-orbital in SMC X-1, there needs to be further in-depth analysis by studying line emissions using high resolution spectra. The variability of these emission lines can constrain the geometry and dynamics of the line-emitting regions in such sources (e.g., LMC X-4; Neilsen et al. 2009). For instance, visibility of some Doppler-shifted lines with super-orbital phases is a direct evidence for the precession of accretion disk. During low (high) super-orbital states when the disk is viewed almost edge-on (face-on), the Doppler-shifted lines originating in the inner accretion disk appear (disappear). On the other hand, if the strength of emission lines do not change with super-orbital phases, the emission lines probably originate in region that subtend a large solid angle to the compact object, possibly the stellar wind (or outer disk). This way, by studying the variability of line fluxes and energies of emission lines we can investigate the physical origin of such super-orbital modulation in SMC X-1. High-resolution spectra can also be used to investigate if the super-orbital modulation is caused by vertical columns in the accretion disk (e.g., EXO 0748-676; Jimenez-Garate et al. 2003). Such analysis are beyond the scope of this paper here and we leave that for future works.

5. SUMMARY

We summarize below the main findings of this work:

- We report broad-band spectral-timing results using sixteen observations of SMC X-1 with *Suzaku* and *NuSTAR*. All individual broad band spectra can be fitted with an absorbed high energy cutoff powerlaw continuum along with a soft blackbody and a weak iron emission line (model 1). Another spectral model with absorbed high energy cutoff powerlaw and a partially ionized absorber (model 2) hint an increase in covering fraction with decreasing intensity of the source. The line equivalent varies from 10 eV in high state to ~ 270 eV in low state.
- Joint spectral fits using model 2 (without black-body component for *NuSTAR*) from all intensity states cannot be explained as being caused by absorption of an otherwise stable source. The change in the normalization of the power-law (factor of ~ 6 in the joint fits) is much larger than expected from changes in the superorbital intensity modulation due to absorption the precessing disk alone. An alternative possibility is the change in the X-ray emission from the source directly that cause such variability.
- Pulsations are detected in all but one *Suzaku* and one *NuSTAR* observation. The detection of pulsation in most of the low-intensity state observations indicate a direct view of the compact object event in the low states in contrary to the prevailing belief of the superorbital modulation being caused by absorption in precessing accretion disk alone.
- The pulse profile shows intensity dependence, the second peak becoming less prominent at lower intensities. These changes in the pulse profiles indicate an intrinsic change in the beaming pattern with the intensity states which could be connected to a change in the accretion rate.
- A putative CRSF is detected at ~ 55 keV in the the brightest *NuSTAR* observations indicates a surface magnetic field of $\sim 4.2 \times 10^{12}$ G for SMC X-1 .
- Period history of SMC X-1 is extended by about 13 years, continues to spin-up. It shows a sudden change in the spin-up rate, perhaps along with a large change in peak luminosity.

ACKNOWLEDGEMENT

The authors would like to thank the reviewer for his/her contributions to the paper in the form of useful comments and suggestions that drastically improved the quality of the paper. This research has made use of data and software provided by the High Energy Astrophysics Science Archive Research Center (HEASARC), which is a service of the Astrophysics Science Division at NASA/GSFC.

Table 2. Best-fit parameters of SMC X-1 during *Suzaku* with model 1 (eqn. 1, see section 3.2 for details). Errors quoted are for 90 per cent confidence range. The observations are arranged in the order of decreasing brightness states with high, medium and low states designated as H, M and L respectively.

	Obs									
	H 10	H 70	H 50	H 80	H 20	H 90	M 30	M 100	L 60	L 40
N_{H1}^a	0.15 ± 0.02	0.15 ± 0.02	0.20 ± 0.02	0.09 ± 0.02	0.22 ± 0.03	0.11 ± 0.04	0.16 ± 0.04	0.14 ± 0.06	0.04 ± 0.04	0.09 ± 0.09
Γ	0.48 ± 0.02	0.49 ± 0.03	0.43 ± 0.03	0.43 ± 0.02	0.50 ± 0.03	0.57 ± 0.03	0.49 ± 0.04	0.22 ± 0.04	-0.42 ± 0.08	-1.05 ± 0.11
E_f	9.4 ± 0.3	9.5 ± 0.3	9.2 ± 0.3	9.2 ± 0.3	10.8 ± 0.3	10.6 ± 0.3	9.9 ± 0.4	8.2 ± 0.4	7.9 ± 0.5	5.7 ± 0.4
Γ_{norm}^b	0.067 ± 0.002	0.052 ± 0.001	0.050 ± 0.001	0.046 ± 0.001	0.038 ± 0.001	0.039 ± 0.002	0.026 ± 0.001	0.011 ± 0.001	0.0005 ± 0.0001	0.0002 ± 0.00001
kT	0.22 ± 0.008	0.22 ± 0.008	0.21 ± 0.007	0.23 ± 0.01	0.21 ± 0.01	0.22 ± 0.02	0.21 ± 0.01	0.17 ± 0.01	0.23 ± 0.02	0.25 ± 0.03
kT_{norm}^c	2.8 ± 0.3	1.7 ± 0.2	2.4 ± 0.3	1.4 ± 0.2	1.4 ± 0.2	0.9 ± 0.2	0.7 ± 0.2	0.3 ± 0.1	0.09 ± 0.02	0.03 ± 0.01
$K\alpha$	6.38 ± 0.05	6.45 ± 0.04	6.43 ± 0.05	6.36 ± 0.06	6.49 ± 0.07	6.36 ± 0.03	6.27 ± 0.08	6.30 ± 0.03	6.41 ± 0.02	6.35 ± 0.05
EW	0.015 ± 0.005	0.026 ± 0.007	0.022 ± 0.005	0.022 ± 0.006	0.013 ± 0.006	0.038 ± 0.011	0.024 ± 0.011	0.038 ± 0.011	0.135 ± 0.022	0.094 ± 0.022
Flux ^d	2.96 ± 0.05	2.70 ± 0.04	2.58 ± 0.02	2.32 ± 0.04	1.99 ± 0.02	1.73 ± 0.01	1.31 ± 0.02	0.67 ± 0.02	0.27 ± 0.01	0.15 ± 0.01
$\chi^2_r/\text{d.o.f}$	1.09/271	1.05/270	1.3/270	1.09/270	1.42/271	1.00/271	1.07/270	1.36/270	1.59/271	1.23/271

^a In units of 10^{22} atoms cm^{-2}

^b In units of photons/keV/ cm^2/s at 1 keV

^c In units of L_{39}/D_{10} where L_{39} is source luminosity in units of 10^{39} erg s^{-1} and D_{10} is the source distance in 10 kpc units.

^d In 1-70 keV, in units of 1×10^{-9} erg $\text{cm}^{-2} \text{s}^{-1}$

Table 3. Best-fit parameters of SMC X-1 during *Suzaku* with model 2 (eqn. 2, see section 3.2 for details). The observations are arranged in the order of decreasing flux states, High (H), medium (M) and low (L) respectively.

	Obs									
	H 10	H 70	H 50	H 80	H 20	H 90	M 30	M 100	L 60	L 40
N_{H1}^a	0.17 ± 0.01	0.17 ± 0.03	0.24 ± 0.03	0.14 ± 0.02	0.26 ± 0.02	0.15 ± 0.04	0.17 ± 0.06	0.15 ± 0.10	0.21 ± 0.07	0.17 ± 0.02
N_{H2}^a	23 ± 8	30 ± 2	48 ± 12	23 ± 8	95 ± 11	23 ± 10	81 ± 9	32 ± 9	41 ± 11	25 ± 7
ξ	1.87 ± 0.66	1.90 ± 0.19	1.89 ± 0.32	1.77 ± 0.34	2.04 ± 0.14	1.85 (-2.92, 0.96)	2.14 ± 0.22	3.06 ± 0.17	1.19 ± 0.36	0.85 ± 0.5
f	0.10 ± 0.02	0.18 ± 0.07	0.25 ± 0.03	0.09 ± 0.01	0.27 ± 0.01	0.03 (-0.01, 0.02)	0.27 ± 0.11	0.44 ± 0.07	0.75 ± 0.04	0.82 ± 0.09
Γ	0.59 ± 0.02	0.65 ± 0.01	0.60 ± 0.02	0.51 ± 0.02	0.60 ± 0.02	0.59 ± 0.03	0.51 ± 0.03	0.59 ± 0.03	0.59 ± 0.07	0.69 ± 0.09
E_f	9.7 ± 0.2	10.1 ± 0.3	9.6 ± 0.2	9.6 ± 0.3	10.4 ± 0.3	9.6 ± 0.3	9.5 ± 0.62	9.8 ± 0.4	10.1 ± 0.9	12 ± 5
Γ_{norm}^b	0.091 ± 0.005	0.069 ± 0.01	0.078 ± 0.004	0.049 ± 0.004	0.063 ± 0.008	0.036 ± 0.006	0.033 ± 0.001	0.015 ± 0.001	0.006 ± 0.003	0.003 ± 0.001
kT	0.21 ± 0.002	0.21 ± 0.01	0.19 ± 0.01	0.20 ± 0.01	0.19 ± 0.01	0.19 ± 0.01	0.21 ± 0.02	0.16 ± 0.03	0.17 ± 0.01	0.17 ± 0.05
kT_{norm}^c	2.92 ± 0.16	1.79 ± 0.26	2.79 ± 0.01	1.67 ± 0.24	1.71 ± 0.30	1.15 ± 0.29	0.77 ± 0.21	0.28 ± 0.32	0.17 ± 0.07	0.05 ± 0.09
$K\alpha$	6.37 ± 0.04	6.46 ± 0.06	6.41 ± 0.06	6.39 ± 0.06	6.52 ± 0.12	6.38 ± 0.04	6.28 ± 0.10	6.32 ± 0.04	6.41 ± 0.03	6.35 ± 0.06
EW	0.014 ± 0.007	0.024 ± 0.006	0.013 ± 0.007	0.020 ± 0.002	0.011 ± 0.006	0.040 ± 0.011	0.015 ± 0.011	0.035 ± 0.012	0.100 ± 0.017	0.053 ± 0.025
Flux ^d	3.62 ± 0.06	2.70 ± 0.07	2.54 ± 0.06	2.51 ± 0.03	2.21 ± 0.05	1.94 ± 0.05	1.43 ± 0.04	0.78 ± 0.02	0.22 ± 0.01	0.17 ± 0.09
Flux ^e	1.44 ± 0.01	1.21 ± 0.01	1.18 ± 0.01	1.16 ± 0.01	1.06 ± 0.01	0.89 ± 0.01	0.66 ± 0.03	0.43 ± 0.02	0.13 ± 0.10	0.10 ± 0.10
$\chi^2_r/\text{d.o.f}$	0.81/267	0.96/267	1.22/267	1.00/267	1.25/268	0.89/268	1.0/268	1.14/267	1.35/267	1.00/268

^a In units of 10^{22} atoms cm^{-2}

^b In units of photons/keV/ cm^2/s at 1 keV

^c In units of $1 \times 10^{-3} L_{39}/D_{10}$ where L_{39} is source luminosity in units of 10^{39} erg s^{-1} and D_{10} is the source distance in 10 kpc units.

^d In 1-70 keV, in units of 1×10^{-9} erg $\text{cm}^{-2} \text{s}^{-1}$

^e In 13-70 keV, in units of 1×10^{-9} erg $\text{cm}^{-2} \text{s}^{-1}$

REFERENCES

- Bildsten L, et al. 1997 *ApJS* 113 367.
 Bozzo E, et al. 2017 *A&A* 606 L10.
 Brumback MC, et al. 2020 *The Astrophysical Journal* 888 125.
 Clarkson W, et al. 2003 *Monthly Notices of the Royal Astronomical Society* 339 447.
 Corbet RHD, & Krimm HA. 2013 *ApJ* 778 45.
 Dage KC, et al. 2019 *MNRAS* 482 337.
 Farrell SA, et al. 2008 *MNRAS* 389 608.
 Fukazawa Y, et al. 2009 *PASJ* 61 17.
 Giménez-García A, et al. 2015 *A&A* 576 A108.
 Gruber DE, & Rothschild RE. 1984 *ApJ* 283 546.
 Harrison FA, et al. 2013 *The Astrophysical Journal* 770 103.
 Hickox RC, et al. 2004 *ApJ* 614 881.
 Hickox RC, & Vrtilek SD. 2005 *ApJ* 633 1064.
 Hu CP, et al. 2017 *ApJ* 844 16.
 Inam SÇ, et al. 2010 *MNRAS* 403 378.
 Jimenez-Garate MA, et al. 2003 *ApJ* 590 432.
 Kahabka P, & Li XD. 1999 *A&A* 345 117.
 Koenigsberger G, et al. 2006 *A&A* 458 513.
 Kotze MM, & Charles PA. 2012 *MNRAS* 420 1575.
 Koyama K, et al. 2007 *PASJ* 59 23.

Table 4. Best-fit parameters of SMC X-1 during *NuSTAR* observations with model 2 minus the black-body component (see text in section 3.2 for details). Errors quoted are for 90 per cent confidence range. The observations are separated into three states H, M, L for high, medium and low states respectively.

	OBSID					
	H	H	H	M	L	L
	30202004008	10002013003	30202004002	30202004004	10002013001	30202004006
N_{H1}^a	0.40 \pm 0.11	0.46	0.46	0.46	2.0 \pm 0.15	4.3 \pm 0.2
N_{H2}^a	22 \pm 2	23	11	43	51 \pm 0.77	85 \pm 2
ξ	1.36 \pm 0.30	2.52 \pm 0.07	0.19 \pm 0.30	1.22 \pm 0.17	1.21 \pm 0.10	0.71 \pm 0.11
f	0.22 \pm 0.05	0.13 \pm 0.01	0.17 \pm 0.01	0.34 \pm 0.01	0.75 \pm 0.03	0.73 \pm 0.01
Γ	0.86 \pm 0.01	0.85 \pm 0.01	0.85 \pm 0.01	0.85 \pm 0.01	0.84 \pm 0.02	0.85 \pm 0.01
E_f	11.1 \pm 0.1	11.05 \pm 0.12	11.65 \pm 0.11	10.98 \pm 0.08	8.69 \pm 0.06	7.9 \pm 0.4
PL_{norm}^b	0.119 \pm 0.002	0.104 \pm 0.005	0.091 \pm 0.010	0.077 \pm 0.001	0.023 \pm 0.002	0.021 \pm 0.004
$K\alpha$	6.44 \pm 0.06	6.50 \pm 0.05	6.42 \pm 0.07	6.56 \pm 0.07	6.38 \pm 0.03	6.32 \pm 0.04
EW	0.023 \pm 0.005	0.030 \pm 0.007	0.105 \pm 0.012 \pm	0.07 \pm 0.01	0.170 \pm 0.015	0.269 \pm 0.114
E_C	52.8 \pm 1.9	51.53 \pm 1.15	53.44 \pm 1.30	-	-	-
σ	9.14 \pm 1.05	9.77 \pm 0.97	11.11 \pm 1.1	-	-	-
τ	10	11.87	16.39 \pm 7.0	-	-	-
Flux ^c (1-70 keV)	2.04 \pm 0.03	2.07 \pm 0.02	1.81 \pm 0.01	1.36 \pm 0.01	0.19 \pm 0.02	0.140 \pm 0.010
Flux ^c (13-70 keV)	0.92 \pm 0.02	0.85 \pm 0.01	0.81 \pm 0.07	0.64 \pm 0.05	0.11 \pm 0.02	0.08 \pm 0.21
$\chi^2_{\nu}/d.o.f$	1.07/697	1.10/696	1.05/698	-	-	-
(without GABS)	1.19/699	1.20/700	1.21/700	1.35/699	1.02/700	1.02/699

^a In units of 10^{22} atoms cm^{-2}

^b In units of photons/keV/ cm^2/s at 1 keV

^c In units of 1×10^{-9} erg cm^{-2} s^{-1}

Larwood J. 1998 MNRAS 299 L32.

Lucke R, et al. 1976 ApJ 206 L25.

Margon B. 1984 ARA&A 22 507.

Mitsuda K, et al. 2007 PASJ 59 1.

Naik S, & Paul B. 2004 A&A 418 655.

Neilsen J, et al. 2004 ApJ 616 L135.

Neilsen J, et al. 2004 The Astrophysical Journal Letters 616 L135.

Neilsen J, et al. 2009 ApJ 696 182.

Ogilvie GI, & Dubus G. 2001 MNRAS 320 485.

Paul B, et al. 2002 ApJ 579 411.

Pike SN, et al. 2019 ApJ 875 144.

Postnov K, et al. 2013 Monthly Notices of the Royal Astronomical Society 435 1147.

Pradhan P, et al. 2018 A&A 610 A50.

Price RE, et al. 1971 ApJ 168 L7.

Raichur H, & Paul B. 2010 MNRAS 401 1532.

Rutten RGM, et al. 1992 A&A 260 213.

Takahashi T, et al. 2007 PASJ 59 35.

Trowbridge S, et al. 2007 ApJ 670 624.

Wojdowski P, et al. 1998 The Astrophysical Journal 502 253.

Zdziarski AA, et al. 2009 in Astrophysics with All-Sky X-Ray Observations, ed. Kawai N, et al. 70.